Atomic and magnetic moment distributions in Fe_2MnSi

1996 J. Phys.: Condens. Matter 8 7771

(http://iopscience.iop.org/0953-8984/8/41/021)

J. Phys.: Condens. Matter **8** (1996) 7771–7784. Printed in the UK

Atomic and magnetic moment distributions in Fe_2MnSi

T Ersez†, S J Kennedy‡ and T J Hicks†

† Department of Physics, Monash University, Clayton, Victoria 3168, Australia

‡ Neutron Scattering Group, ANSTO, PMB 1, Menai, NSW 2234, Australia

Received 8 May 1996, in final form 12 July 1996

Abstract. Polarized neutron diffuse scattering studies made above and below the re-ordering temperature T_R on an Fe_2MnSi crystal have revealed a random atomic arrangement of Mn and Fe atoms. The magnetic disturbance produced by Mn atoms is confined to the substituted sites. There appears to be greater change in the moment difference between Mn and Fe atoms on the Mn predominant B site with change in concentration x_B for $T < T_R$ than for $T > T_R$. Above and below T_R, the moments of Mn and Fe atoms on the Fe predominant A, C sites are very similar.

1. Introduction

Heusler alloys and related intermetallic compounds provide opportunities for the investigation of the effects of chemical order and for detailed understanding of magnetism in metallic systems. The crystal structure of the compounds described in this paper is $L2_1$, which is very similar to the DO_3-type structure of Fe_3Si except that Fe atoms on the B sites are replaced by Mn atoms. The DO_3 structure may be described by a unit cell which consists of four cubic interpenetrating sublattices A, B, C and D with origins at the points (0, 0, 0), (1/4, 1/4, 1/4), (1/2, 1/2, 1/2) and (3/4, 3/4, 3/4).

The compound Fe_2MnSi is a member of the $Fe_{3-x}Mn_xSi$ alloy series, where $0 \leqslant x \leqslant 3$. For $x \sim 1$, Mn atoms begin to enter A and C sites as well as B sites. At room temperature the compound is paramagnetic. Between approximately 65 and 215 K it is ferromagnetic (FM), but below its re-ordering temperature $T_R \sim 65$ K a complex magnetic behaviour exists. Powder neutron diffraction data (Yoon and Booth 1974, 1977, Ziebeck and Webster 1976) have indicated that the manganese atoms are antiferromagnetically ordered with a FM component, whereas the iron atoms remain ferromagnetically aligned, implying a rhombohedral antiferromagnetic (AFM) ordering of the magnetic moments on the B sublattice. The moments on Mn B site atoms cant toward [111] directions; the degree of canting increases as the temperature is reduced, giving both FM and AFM components to the moments. The absence of the $\frac{1}{2}(111)$ reflection in the powder neutron diffraction data recorded below T_R has indicated the antiferromagnetically aligned moments to be directed along the [111] direction. Recent neutron polarization analysis investigations carried out on an Fe_2MnSi single-crystal specimen at 36 K have confirmed the above-assumed relatively simple structure with orthogonality between the FM and AFM directions below T_R for $Fe_{3-x}Mn_xSi$ alloys (Ersez *et al* 1995a).

Clearly, the natures of the magnetic interactions and moment formation in Fe_2MnSi are complex. To provide further insight into the nature of these magnetic properties low-temperature polarized neutron diffuse scattering measurements have been made on a

0953-8984/96/417771+14$19.50

Fe_2MnSi single crystal. Fitting of a model to the magnetic diffuse scattering will allow the average magnetic moment distribution to be determined in this alloy.

Considerable developments have been made in analysing diffusely scattered intensity and most of the experimental and theoretical investigations have largely been confined to binary systems. As a result a larger body of data exists for binary systems compared with multicomponent systems. Most quantitative studies of diffuse x-ray or neutron scattering to reveal local atomic arrangements, such as clustering or local order, have been carried out on metallic binary alloys which have one atom per lattice point, but in the Fe_2MnSi compound three of the sites have combinations of Fe and Mn atoms. No direct determinations of magnetic moment distributions have been made on solid solutions with disorder on more than one sublattice. However, Hayakawa and Cohen (1975) have derived general equations for diffuse scattering from materials with multiple sublattices and given examples for determining atomic short-range order. Cenedese *et al* (1984) adopted the general theory of Hayakawa and Cohen (1975) and also, following the methods of Borie and Sparks (1971) (and Tibbals (1975) in the case of x-ray diffuse scattering), were able to determine the local atomic arrangement in a ternary alloy of $Fe_{0.56}Cr_{0.21}Ni_{0.23}$. Three independent neutron diffuse scattered intensities were needed to measure the Fe–Ni, Fe–Cr and Ni–Cr pair correlations. These were obtained by three experiments on three crystals with identical chemical but different isotopic compositions.

Owing to the availability of synchrotron radiation, there exists the possibility of analysing local order in multicomponent alloys. By using only one single crystal, and x-ray diffuse scattering, and choosing wavelengths close to the absorption edges of an element it is possible to determine pair correlations in a ternary alloy (Cenedese *et al* 1984). However, with magnetic alloys the magnetic order also needs to be considered. Recently, Johnson *et al* (1996) implemented a first-principles theory of short-range order (sro) in high-temperature, disordered, multicomponent alloys which allows determination of the electronic origins of this sro in chemically (homogeneously) random alloys. They also mention that independent sro parameters can be determined experimentally by varying the energies in anomalous x-ray experiments. Thus, a combination of neutron scattering and synchrotron radiation experiments appear to be necessary to determine the individual atomic arrangements and magnetic moment distributions and average moments of each of the species of a multicomponent magnetic specimen.

In this study, only polarized neutron scattering measurements were made above and below T_R for the Fe_2MnSi crystal and the results and analysis are given in the following sections, in which the equations that were derived to model the two-component disordered data are presented together with the average atomic and magnetic moment distributions determined.

2. Experimental details

The specimen was in the shape of a disc (diameter 10 mm and thickness 7 mm), with its axis along [100]. The lattice parameter and composition were checked using x-ray diffraction and electron microprobe analysis.

Following the mounting of the crystal (its $[1\bar{1}0]$ axis close to the vertical direction) within a c-shaped permanent magnet in a saturating vertical field of 7 kOe, polarized neutron experiments were performed at 37 K (AFM region) and 100 K (FM region) on the LONGPOL spectrometer at the HIFAR Research Reactor (Lucas Heights, Australia). Monochromatic neutrons with a wavelength of 3.6 Å were used which pass through a magnetized iron polarizing filter. The iron analysing filter was removed for this experimental

set-up and measurements were performed around the ferromagnetic (111) Bragg reflection. A time-of-flight (TOF) experiment was carried out, measuring elastic scattering, by pulsing the spin flipper (before the sample position) with a pseudo-random sequence, and cross-correlating the resulting time sequence at each of the eight detectors with that impressed on the spin flipper (Davis *et al* 1982, Cussen *et al* 1992).

Background measurements were made by carefully matching the sample attenuation with an indium sample of approximately the same dimensions. The background was subtracted from the data before carrying out further analysis. Relative detector efficiency and absolute cross-section calibration were performed by substituting a vanadium sample of similar dimensions and repeating the experiments.

Multiple-scattering and absorption corrections were made by using the analytical techniques of Sears (1975), in which the multiple scattering was appropriately apportioned between flipper on and off events.

3. Theory

The compound Fe_2MnSi cannot be regarded as a usual ternary system with single atomic species on each of the three different sublattice sites (A = C, B and D). It can be considered to be more like a pseudo-binary alloy system with two different atomic species present together on each of the two different sublattice sites (A = C and B). Thus, there exist two different defects on each of the sites. The D site is completely occupied by Si atoms, which we assume carry no magnetic moment.

Following Hayakawa and Cohen (1975) the nuclear diffuse cross-section for scattering from multiple sublattices can be written as

$$\left(\frac{\mathrm{d}\sigma}{\mathrm{d}\Omega}\right) = \sum_m \sum_n \sum_\mu \sum_\nu \sum_j \sum_{i>j} x_\mu^i x_\nu^j (b_i - b_j)^2 \alpha_{\mu\nu}^{ij} S_{\mu\nu} A_{mn} \tag{1}$$

where: m, n = lattice indices; μ, ν = sublattice indices; x_μ^i, x_ν^j = sublattice fractions of atoms i and j respectively; b_i, b_j = scattering lengths of atoms i and j respectively; $\alpha_{\mu\nu}^{ij}$ = sro parameters for i and j atoms at the sublattices μ and ν; $S_{\mu\nu} = \mathrm{e}^{\mathrm{i}\boldsymbol{\kappa}\cdot(\boldsymbol{r}_\mu - \boldsymbol{r}_\nu)}$; $A_{mn} = \mathrm{e}^{\mathrm{i}\boldsymbol{\kappa}\cdot(\boldsymbol{r}_m - \boldsymbol{r}_n)}$; $\boldsymbol{r}_m$, $\boldsymbol{r}_n$ = the positional vectors of the mth and nth lattice point with respect to an arbitrary origin; $\boldsymbol{r}_\mu$, $\boldsymbol{r}_\nu$ = sublattice vectors of the μth and νth sublattice with respect to the lattice points.

In the case of Fe_2MnSi, equation (1) becomes

$$\begin{aligned}\left(\frac{\mathrm{d}\sigma}{\mathrm{d}\Omega}\right) = \sum_m \sum_n [&x_B^{Fe} x_B^{Mn} \alpha_{BB}^{FeMn}(\boldsymbol{r}_m - \boldsymbol{r}_n) + x_{A,C}^{Fe} x_{A,C}^{Mn} \alpha_{(A,C)^2}^{FeMn}(\boldsymbol{r}_m - \boldsymbol{r}_n) \\ &+ x_B^{Fe} x_{A,C}^{Mn} \alpha_{B,(A,C)}^{FeMn}(\boldsymbol{r}_m - \boldsymbol{r}_n)(\mathrm{e}^{\mathrm{i}\boldsymbol{\kappa}\cdot(\boldsymbol{r}_A - \boldsymbol{r}_B)} + \mathrm{e}^{\mathrm{i}\boldsymbol{\kappa}\cdot(\boldsymbol{r}_C - \boldsymbol{r}_B)}) \\ &+ x_{A,C}^{Fe} x_B^{Mn} \alpha_{B,(A,C)}^{FeMn}(\boldsymbol{r}_m - \boldsymbol{r}_n)(\mathrm{e}^{\mathrm{i}\boldsymbol{\kappa}\cdot(\boldsymbol{r}_A - \boldsymbol{r}_B)} + \mathrm{e}^{\mathrm{i}\boldsymbol{\kappa}\cdot(\boldsymbol{r}_C - \boldsymbol{r}_B)})] \\ &\times (b_{Fe} - b_{Mn})^2 \mathrm{e}^{\mathrm{i}\boldsymbol{\kappa}\cdot(\boldsymbol{r}_m - \boldsymbol{r}_n)}.\end{aligned} \tag{2}$$

Equation (2) can be written in terms of *all* of the atom separations $\boldsymbol{r}$ as follows:

$$\begin{aligned}\left(\frac{\mathrm{d}\sigma}{\mathrm{d}\Omega}\right) = N \sum_{\boldsymbol{r}} \Bigg[&\frac{1}{4} x_B^{Fe} x_B^{Mn} \alpha_{B,B}^{FeMn}(\boldsymbol{r}) + \frac{1}{2} x_{A,C}^{Fe} x_{A,C}^{Mn} \alpha_{(A,C),(A,C)}^{FeMn}(\boldsymbol{r}) \\ &+ \frac{1}{4} x_B^{Fe} x_{A,C}^{Mn} \alpha_{B,(A,C)}^{FeMn}(\boldsymbol{r}) + \frac{1}{2} x_{A,C}^{Fe} x_B^{Mn} \alpha_{(A,C),B}^{FeMn}(\boldsymbol{r}) \Bigg](b_{Fe} - b_{Mn})^2 \mathrm{e}^{\mathrm{i}\boldsymbol{\kappa}\cdot\boldsymbol{r}}\end{aligned} \tag{3}$$

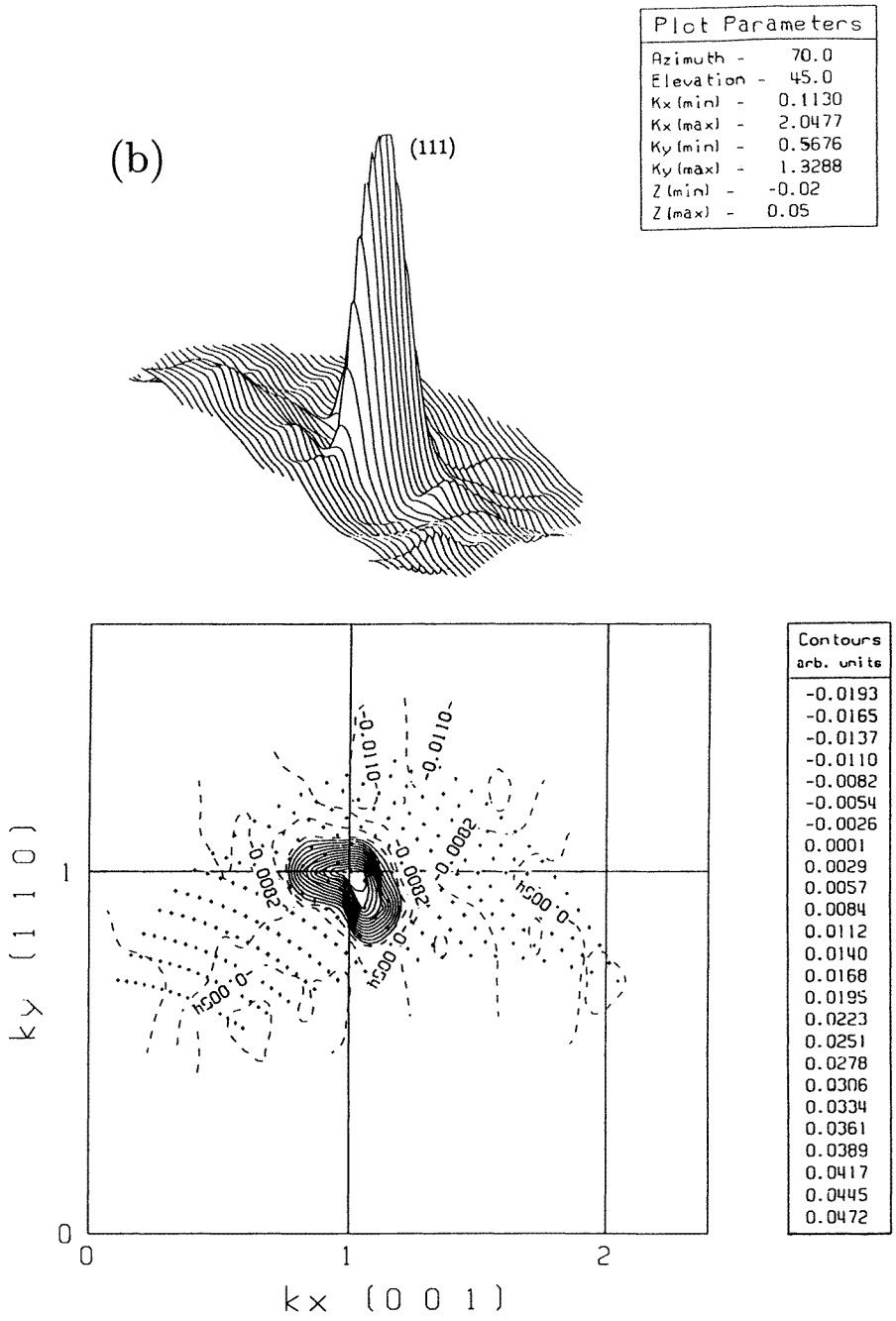

Figure 1. (a) Surface and contour plots of the raw difference between spin-up and spin-down scattering at 37 K, which were normalized to a maximum value of 0.05 to enhance the negative difference cross-sections. (b) Surface and contour plots of the raw difference between spin-up and spin-down scattering at 100 K, which were normalized to a maximum value of 0.05 to enhance the negative difference cross-sections.

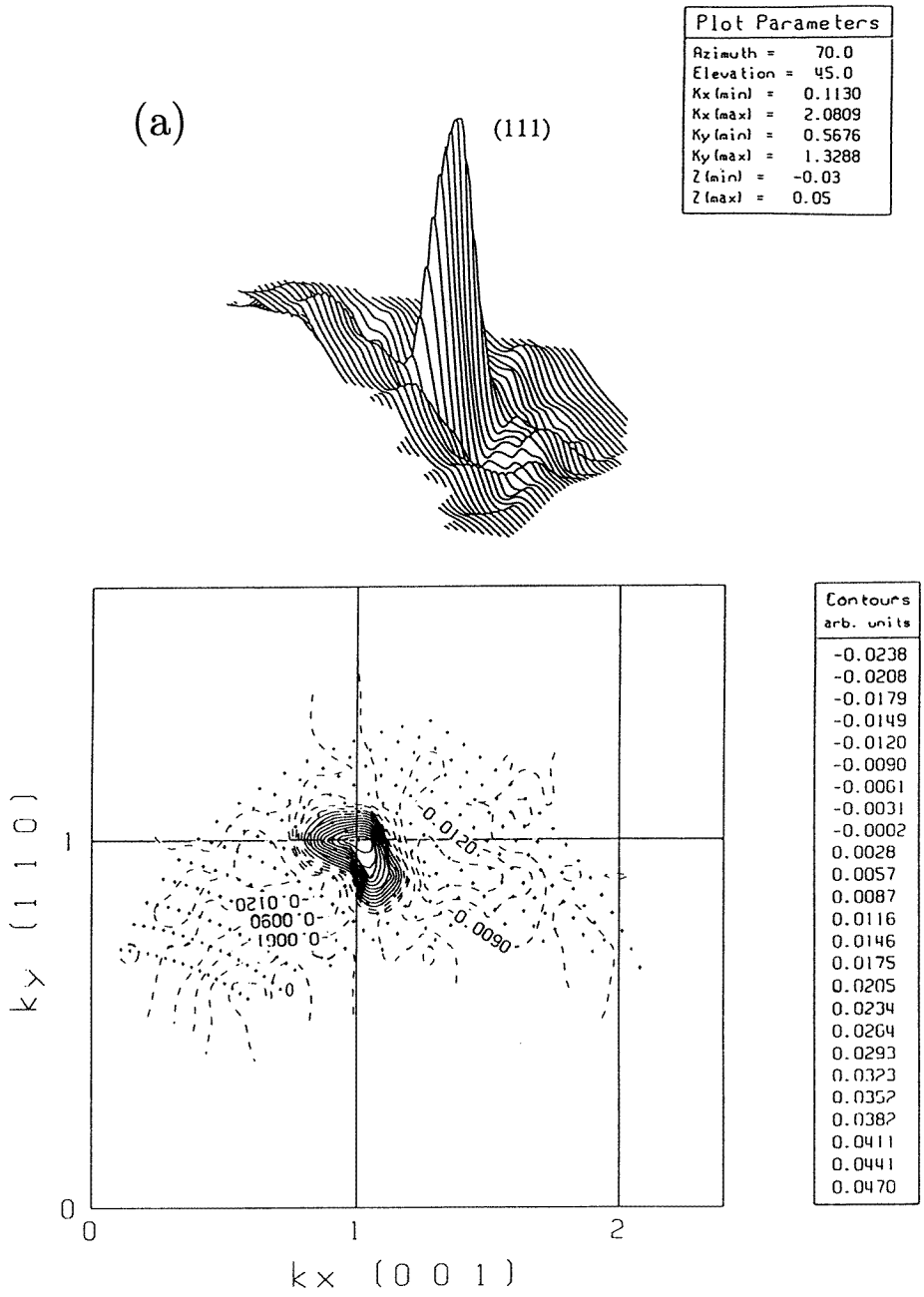

Figure 1. (Continued)

where N is the total number of atom sites and it is understood that not all terms will contribute for each $\boldsymbol{r}$. For instance, considering first-nearest neighbours only, the cross-terms connecting sublattice B and A, C will contribute.

The Laue monotonic scattering cross-section for Fe_2MnSi (adapted from the Laue monotonic scattering expression for a multicomponent system given by Hayakawa and Cohen 1975) is given by

$$\left(\frac{\mathrm{d}\sigma}{\mathrm{d}\Omega}\right) = (x_B^{Mn}x_B^{Fe} + 2x_{A,C}^{Mn}x_{A,C}^{Fe})[b_{Fe} - b_{Mn}]^2 \tag{4}$$

where x_B^{Mn}, x_B^{Fe}, $x_{A,C}^{Mn}$ and $x_{A,C}^{Fe}$ are the Mn and Fe sublattice fractions of 0.88, 0.12, 0.06 and 0.94 respectively. Also, from the known scattering lengths of Mn and Fe (Sears 1984), $[b_{Fe} - b_{Mn}]^2 = (1.327)^2$ b. Therefore, the Laue monotonic scattering cross-section in equation (4) has a value of $\mathrm{d}\sigma/\mathrm{d}\Omega \sim 0.385$ b/formula unit.

A simple model can also be adopted for the magnetic diffuse scattering. On sublattice B the substitution of an Fe for a Mn atom can be regarded as resulting in a change of moment $m_B(\boldsymbol{r})$ where $m_B(0)$ is the defect on the substituted site and there are changes of moment at all sites $\boldsymbol{r}$ (irrespective of sublattice). These changes of moment superpose where they overlap, i.e., the total moment defect at $\boldsymbol{r}$ is the sum of that due to all Fe substituted for Mn atoms nearby. Similarly, $m_{A,C}(\boldsymbol{r})$ is defined to represent the defect caused by the substitution of a Mn for an Fe atom on sublattices A and C. Each magnetic defect can then be treated as a moment cloud, whose form factor multiplied by the total moment is $M_B(\boldsymbol{\kappa})$ and $M_{A,C}(\boldsymbol{\kappa})$ for the respective sublattices.

The magnetic diffuse cross-section, analogous to equation (3), can be written as follows:

$$\begin{aligned}\left(\frac{\mathrm{d}\sigma}{\mathrm{d}\Omega}\right) = N\left(\frac{e^2\gamma}{2mc^2}\right)^2 f^2(\boldsymbol{\kappa}) \sum_{\boldsymbol{r}}\Bigg[&\frac{1}{4}x_B^{Fe}x_B^{Mn}\alpha_{B,B}^{FeMn}(\boldsymbol{r})M_B^2(\boldsymbol{\kappa}) \\ &+ \frac{1}{2}x_{A,C}^{Fe}x_{A,C}^{Mn}\alpha_{(A,C),(A,C)}^{FeMn}(\boldsymbol{r})M_{A,C}^2(\boldsymbol{\kappa}) \\ &+ \left(\frac{1}{4}x_B^{Fe}x_{A,C}^{Mn}\alpha_{B,(A,C)}^{FeMn}(\boldsymbol{r}) + \frac{1}{2}x_{A,C}^{Fe}x_B^{Mn}\alpha_{(A,C),B}^{FeMn}(\boldsymbol{r})\right)M_B(\boldsymbol{\kappa})M_{A,C}(\boldsymbol{\kappa})\Bigg]\mathrm{e}^{\mathrm{i}\boldsymbol{\kappa}\cdot\boldsymbol{r}}\end{aligned} \tag{5}$$

where $e^2\gamma/2mc^2 = -0.269 \times 10^{-12}$ cm/μ_B; $f(\boldsymbol{\kappa})$ is the atomic form factor of both Fe and Mn; $\boldsymbol{\kappa}$ is the neutron scattering vector; $M_B(0)$ and $M_{A,C}(0)$ are $\mathrm{d}\overline{m}_B/\mathrm{d}x_B$ and $\mathrm{d}\overline{m}_{A,C}/\mathrm{d}x_{A,C}$ respectively (Marshall 1968); $\overline{m}_B$ and $\overline{m}_{A,C}$ describe the average moments on the B and A, C sublattices respectively.

4. Results and discussion

From measurements of flipper on and off intensities for the (111) Bragg peak at temperatures $T = 37$ and 100 K and using the values of 1.02 μ_B and 1.4 μ_B for the average moments on the B sites at each of these temperatures (as reported by Yoon and Booth 1977, Ziebeck and Webster 1976, Miles 1991) and also using the magnetic form factors of Fe^{2+} and Mn^{2+} from Watson and Freeman (1961), the polarizations were determined as 41% ($T = 37$ K) and 34.8% ($T = 100$ K).

Diffuse scattering was observed around the (111) Bragg peak at both temperatures of 37 and 100 K. The difference between raw spin-up and spin-down scattering for the two temperatures is given in figures 1(a) and 1(b), which show the difference diffuse and difference Bragg scattering at (111) to be of opposite sign for both temperature settings, with a negative diffuse peak around a positive Bragg peak. In comparing figures 1(a) and 1(b) the positive contour region at 100 K is seen to be broader than at a temperature of 37 K. Furthermore, the polarized neutron scattering measurements carried out in this study

have shown that the negative diffuse scattering is more pronounced for a $Fe_{2.45}Mn_{0.55}Si$ crystal. As mentioned previously (Ersez *et al* 1995b), the sign difference for the diffuse and Bragg scattering at the (111) position is consistent with a loss of moment on the B site with addition of manganese and the nuclear structure factor being already negative at this composition.

4.1. Nuclear diffuse scattering

Specific to the Fe_2MnSi alloy, the spin-up and spin-down diffuse cross-section expressions describing the atomic arrangements and magnetic moment distributions for the A, C and B sites can be written as follows:

$$\left(\frac{d\sigma}{d\Omega}\right)^{\uparrow\downarrow} = \left[\left(\frac{e^2\gamma}{2mc^2}\right) f(\boldsymbol{\kappa}) m^*(\boldsymbol{\kappa}) \pm b^*(\boldsymbol{\kappa})\right]\left[\left(\frac{e^2\gamma}{2mc^2}\right) f(\boldsymbol{\kappa}) m(\boldsymbol{\kappa}) \pm b(\boldsymbol{\kappa})\right] \tag{6}$$

where: $b(\boldsymbol{\kappa})b(-\boldsymbol{\kappa})$ = nuclear diffuse scattering cross-section given in equation (3); and $(e^2\gamma/2mc^2)^2 f^2(\boldsymbol{\kappa})m(\boldsymbol{\kappa})m(-\boldsymbol{\kappa})$ = magnetic diffuse scattering cross-section given in equation (5).

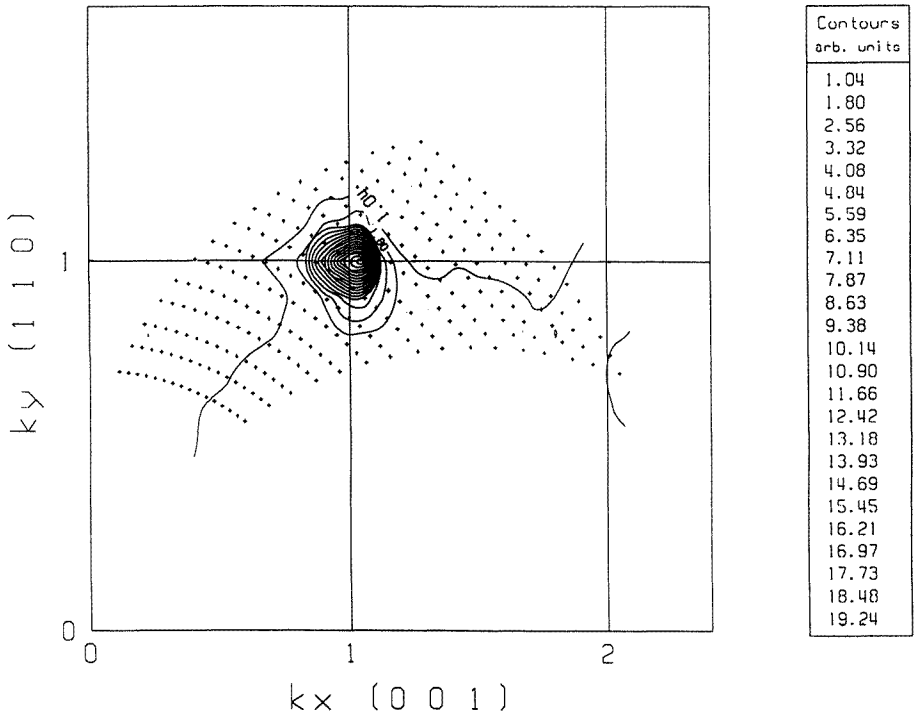

Figure 2. A contour plot of the experimentally determined nuclear short-range-order function $\Xi(\boldsymbol{\kappa})$ at 100 K, normalized to a maximum value of 20.0 to enhance the diffuse region.

Since an overall centrosymmetric symmetry exists between the sublattice sites ($\mu\nu = \nu\mu$) in the crystallographic structure of Fe_2MnSi, $b(\boldsymbol{\kappa})$ and $m(\boldsymbol{\kappa})$ can be considered to be

real. Thus $b(\boldsymbol{\kappa}) = b(-\boldsymbol{\kappa})$ and $m(\boldsymbol{\kappa}) = m(-\boldsymbol{\kappa})$ and equation (6) becomes

$$\left(\frac{\mathrm{d}\sigma}{\mathrm{d}\Omega}\right)^{\uparrow\downarrow} = \left[\left(\frac{e^2\gamma}{2mc^2}\right) f(\boldsymbol{\kappa}) m(\boldsymbol{\kappa}) \pm b(\boldsymbol{\kappa})\right]^2. \tag{7}$$

From the total and difference cross-sections of equation (7) $b(\boldsymbol{\kappa})$ and $m(\boldsymbol{\kappa})$ can be determined. The nuclear sro function $\Xi(\boldsymbol{\kappa})$ describes the occupation of B and A, C sites and for a cubic-structured single crystal has the following form:

$$\Xi(\boldsymbol{\kappa}) = \frac{b^2(\boldsymbol{\kappa})}{(x_B^{Fe} x_B^{Mn} + 2x_{A,C}^{Fe} x_{A,C}^{Mn})(b_{Fe} - b_{Mn})^2} = \sum_{\boldsymbol{R}_i} \alpha_i \mathrm{e}^{\mathrm{i}\boldsymbol{\kappa}\cdot\boldsymbol{R}_i} \tag{8}$$

where $b^2(\boldsymbol{\kappa})$, as described previously, represents the nuclear diffuse scattering cross-section; α_i are the Cowley sro parameters (Cowley 1950); $\boldsymbol{R}_i$ are the radius vectors from the defect atom to neighbours in the ith shell; and $\boldsymbol{\kappa}$ as defined previously.

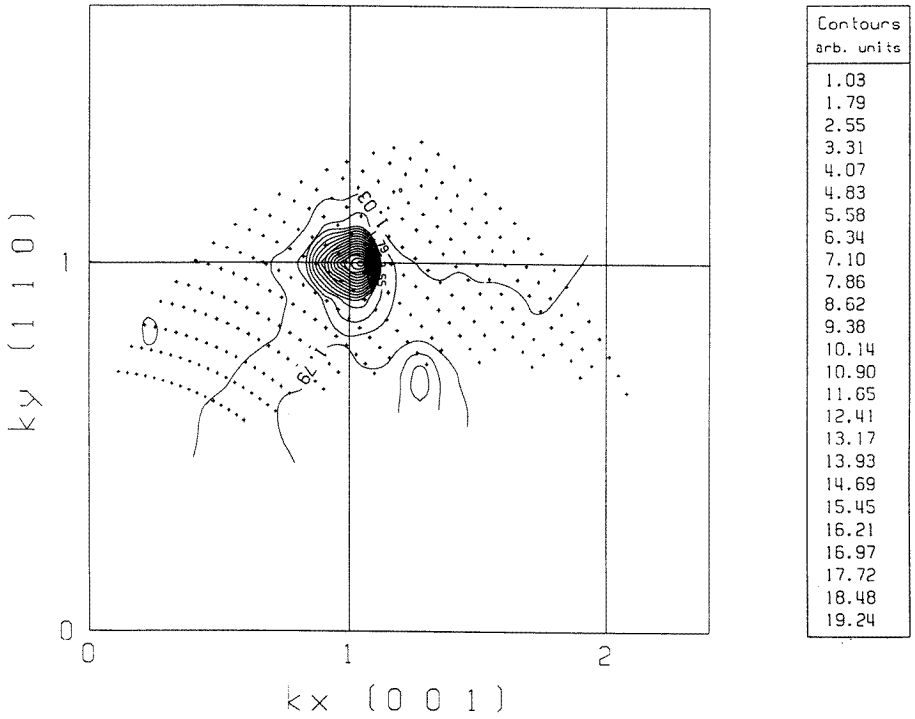

Figure 3. A contour plot of the experimentally determined nuclear short-range-order function $\Xi(\boldsymbol{\kappa})$ at 37 K, normalized to a maximum value of 20.0 to enhance the diffuse region.

4.1.1. $T(=100\ K) > T_R$. The experimental cross-section data were converted to values of $\Xi(\boldsymbol{\kappa})$ using equations (7) and (8) and are presented in the contour plot shown in figure 2. These results were then least-squares fitted to equation (8) using the Cowley model to fit the diffuse scattering data, and the (111) Bragg peak intensity was fitted with a bivariate gaussian distribution. The fit was made with parameters α_0 to α_2 (i.e., up to the second nn). Extending the fit beyond the 2nd nn did not significantly improve the fit. The fitted value of α_0 compares well, within standard error, with the theoretical value of $\alpha_0 = 1$, which is also

Table 1. Cowley short-range-order parameters for Fe_2MnSi.

	Cowley sro parameters, α_i	Fit value	Standard error
$T = 100$ K	α_0	0.98	0.09
	α_1	−0.01	0.05
	α_2	−0.01	0.02
$T = 37$ K	α_0	1.05	0.09
	α_1	−0.06	0.05
	α_2	−0.001	0.02

an additional check on our model, further confirming the accuracy of our calibration. From the definition of $b^2(\boldsymbol{\kappa})$ given in equations (3) and (6) and the nn configurations for each of the sites given in table 1, only certain individual α-pair site parameters can be extracted. Since the 2nd nn of B site atoms are Si atoms on the D sites, $\alpha_2 \equiv 0.113\alpha^{FeMn}_{(A,C),(A,C)}$. Therefore, $\alpha^{FeMn}_{(A,C),(A,C)} = -0.08$. In the case of 1st nn, $\alpha_1 \equiv 0.007\alpha^{FeMn}_{B,(A,C)} + 1.654\alpha^{FeMn}_{(A,C),B}$ and $\alpha^{FeMn}_{B,(A,C)}$ and $\alpha^{FeMn}_{(A,C),B}$ cannot be determined individually from only the information that is currently available. The α_1- and $\alpha^{FeMn}_{(A,C),(A,C)}$-terms have large errors associated with them and α_1 is small in value, which suggests a possible random atomic arrangement at this temperature in this alloy.

4.1.2. $T(=37\ K) < T_R$. Similarly, the experimental cross-section data obtained in this temperature regime were also converted to values of $\Xi(\boldsymbol{\kappa})$ using equations (7) and (8), which are presented in the contour plot shown in figure 3. These results were also least-squares fitted to equation (8) using the Cowley model to fit the diffuse scattering data and a bivariate gaussian distribution was used to fit the (111) Bragg peak intensity. This fitting was made with parameters α_0 to α_2 (i.e., up to 2nd nn). Extending the fit beyond the 2nd nn did not significantly improve the fit. The results of the fittings are also given in table 1 and the Cowley sro parameters are similar at the two temperatures, as would be expected. There is reasonable agreement also, within standard error, at this temperature between the fit value for α_0 and the theoretical value of $\alpha_0 = 1$. The individual pair site parameter $\alpha^{FeMn}_{(A,C),(A,C)}$ was determined as having a value of approximately -0.006. The α_1- and $\alpha^{FeMn}_{(A,C),(A,C)}$-parameters, like those at $T = 100$ K, have large errors associated with them and at this temperature $\alpha^{FeMn}_{(A,C),(A,C)}$ is close to zero in value. These results, as well, suggest a possible random atomic arrangement at $T = 37$ K and indicate that any variations in the diffuse scattering intensity are due to statistical fluctuations in the data. Similarly, Co atoms have been reported to substitute randomly for Fe(A, C) atoms exclusively in Fe_3Si to form the well ordered Fe_2CoSi alloy (Niculescu *et al* 1983).

4.2. Magnetic diffuse scattering

4.2.1. $T(=100\ K) > T_R$. Fitting of a model to the magnetic diffuse scattering allows a determination of the average magnetic moment distributions in the Fe_2MnSi compound. The magnetic diffuse scattering function, $\mathcal{M}(\boldsymbol{\kappa})$, which is related to the magnetic diffuse

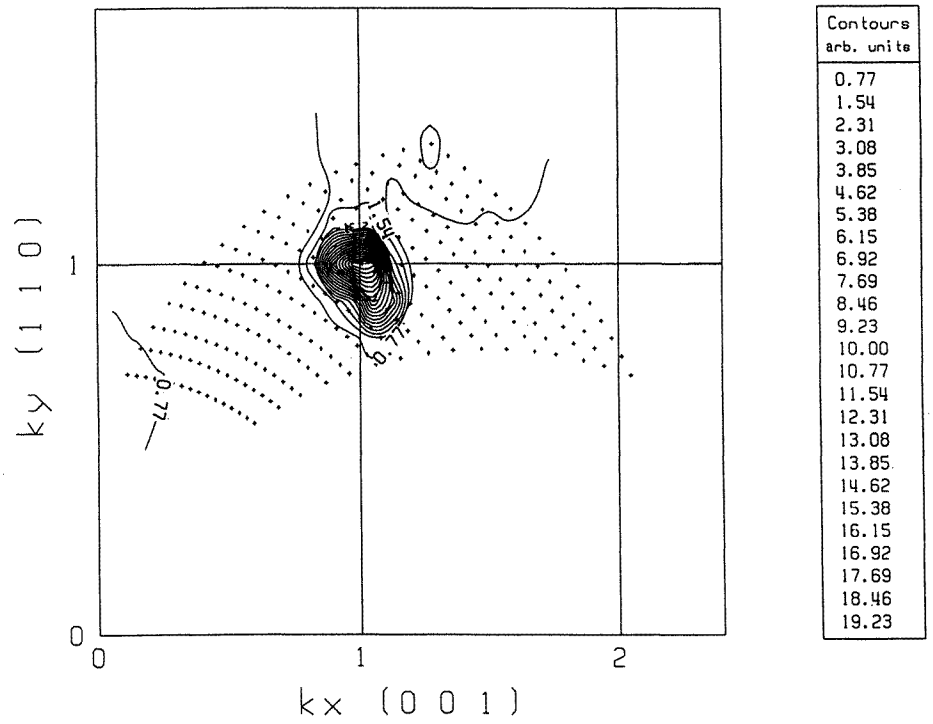

Figure 4. A contour plot of the experimentally determined Fourier transform of the magnetic moment defect distribution, $\mathcal{M}(\boldsymbol{\kappa})$ at 100 K, normalized to a maximum value of 20.0 to enhance the diffuse region.

Table 2. Moment defect parameters (μ_B/formula unit).

	m_i	Fit value	Standard error
$T = 100$ K	m_0	1.4	0.4
	m_1	−0.3	0.7
$T = 37$ K	m_0	1.8	0.4
	m_1	−0.1	0.6

scattering cross-section of equation (5), is given by

$$\mathcal{M}(\boldsymbol{\kappa}) = \frac{m^2(\boldsymbol{\kappa})}{(x_B^{Fe}x_B^{Mn} + 2x_{A,C}^{Fe}x_{A,C}^{Mn})}. \tag{9}$$

Values of $\mathcal{M}(\boldsymbol{\kappa})$ were determined from the experimental cross-sections, using equations (7) and (9), and are shown in figure 4 as a contour plot. This set of $\mathcal{M}(\boldsymbol{\kappa})$-data was least-squares fitted to equation (9) together with a bivariate gaussian distribution for the (111) Bragg peak, to yield the moment defect parameters m_i. The $\mathcal{M}(\boldsymbol{\kappa})$-function and bivariate gaussian distribution functions are independent and the diffuse scattering data were reliably fitted with parameters m_0 and m_1 (see table 2). Using extra parameters did not lead to significant improvement in the fit. Having already obtained fit values for the nuclear sro parameters, given in the previous section, from equation (5) and table 1, we can

determine $M_B(\boldsymbol{\kappa})$ and $M_{A,C}(\boldsymbol{\kappa})$. In the case of m_0, M_B and $M_{A,C}$ can be considered to be $\boldsymbol{\kappa}$-independent, and from equation (5) the following expression is obtained:

$$\begin{aligned} &x_B^{Fe}x_B^{Mn}M_B^2 + 2x_{A,C}^{Fe}x_{A,C}^{Mn}M_{A,C}^2 = 1.4 \\ &0.106M_B^2 + 0.113M_{A,C}^2 = 1.4. \end{aligned} \tag{10}$$

Since the moment defect parameter, m_1, has a large standard error and its fit value is small it can be assumed that this first Fourier component is due entirely to the sro α-parameters. The small variations observed in the diffuse scattering (figure 4) were most probably due to statistical fluctuations in the data and could be reasonably fitted with a constant term m_0. Therefore, from equation (5),

$$\begin{aligned} &[x_B^{Fe}x_{A,C}^{Mn}\alpha_{B,(A,C)}^{FeMn}(\boldsymbol{r}) + 2x_{A,C}^{Fe}x_B^{Mn}\alpha_{(A,C),B}^{FeMn}(\boldsymbol{r})]M_BM_{A,C} = -0.3 \\ &-0.01M_BM_{A,C} = -0.3. \end{aligned} \tag{11}$$

However, this results in non-real solutions if the terms M_B or $M_{A,C}$ from equation (11) are substituted into equation (10), but from the observed site moments of Yoon and Booth (1977), $\mathrm{d}M_{A,C}/\mathrm{d}x_{A,C} \sim 0\ \mu_B$/f.u. Using this information and the fact that the fit value -0.3 has a large standard error associated with it, suggests here that $M_{A,C} \equiv \mathrm{d}M_{A,C}/\mathrm{d}x_{A,C} \sim 0$ μ_B/f.u. and therefore, $M_B \equiv \mathrm{d}M_B/\mathrm{d}x_B \sim \pm 3.6\ \mu_B$/f.u. Due to the decrease in Bragg peak intensity on going from above T_R to below T_R and the fact that the magnetic intensity above and below T_R decreases with increasing Mn concentration on B sites, the solution should be of negative sign, i.e., $\mathrm{d}M_B/\mathrm{d}x_B \sim -3.6 \pm 0.5\ \mu_B$/f.u.

This value of $\mathrm{d}M_B/\mathrm{d}x_B$ compares quite well with $\mathrm{d}M_B/\mathrm{d}x_B \sim -4.2\ \mu_B$/f.u. deduced from table 5 (for site occupancies) and table 7 (for observed site moments) of Yoon and Booth (1977). (NB The neutron diffraction measurements of Yoon and Booth (1977) were carried out at 77 K for alloy concentrations $x = 0.75$ to 1.5 and the C site labelling used by them refers to the B site in this study.)

The neutron diffraction results have shown that the A and C site moments remain constant at $\sim 0.4\ \mu_B$ in the concentration range $0.75 \leqslant x \leqslant 1.75$, i.e., there is no change in the moment on these sites with change in overall Mn concentration x. Additionally, the term $\mathrm{d}M_{A,C}/\mathrm{d}x_{A,C}$ here indicates that there does not seem to be much difference between the moments of Mn and Fe atoms residing on the A, C sites with change in concentration on the A, C sites.

4.2.2. $T(=37\ K) < T_R$. By means of equations (7) and (9), values of $\mathcal{M}(\boldsymbol{\kappa})$ in the re-ordering regime were determined from the experimental cross-sections obtained at 37 K and are presented as a contour plot in figure 5. This set of $\mathcal{M}(\boldsymbol{\kappa})$-data was also least-squares fitted to equation (9) together with a bivariate gaussian distribution for the (111) Bragg peak, to yield the moment defect parameters m_i. The diffuse scattering data in this temperature regime were also reliably fitted with parameters m_0 and m_1 and are listed as well in table 2. Employing more parameters in the fitting procedure did not lead to significant improvement in the fit. Here M_B and $M_{A,C}$ are also considered to be $\boldsymbol{\kappa}$-independent, since once again the moment defect parameter, m_1, is small in value and has a larger standard error than its fit value, and it can be assumed that the first Fourier component is due entirely to the sro α-parameters. From equation (5) the following expression is obtained in the case of m_0:

$$\begin{aligned} &x_B^{Fe}x_B^{Mn}M_B^2 + 2x_{A,C}^{Fe}x_{A,C}^{Mn}M_{A,C}^2 = 1.8 \\ &0.106M_B^2 + 0.113M_{A,C}^2 = 1.8 \end{aligned} \tag{12}$$

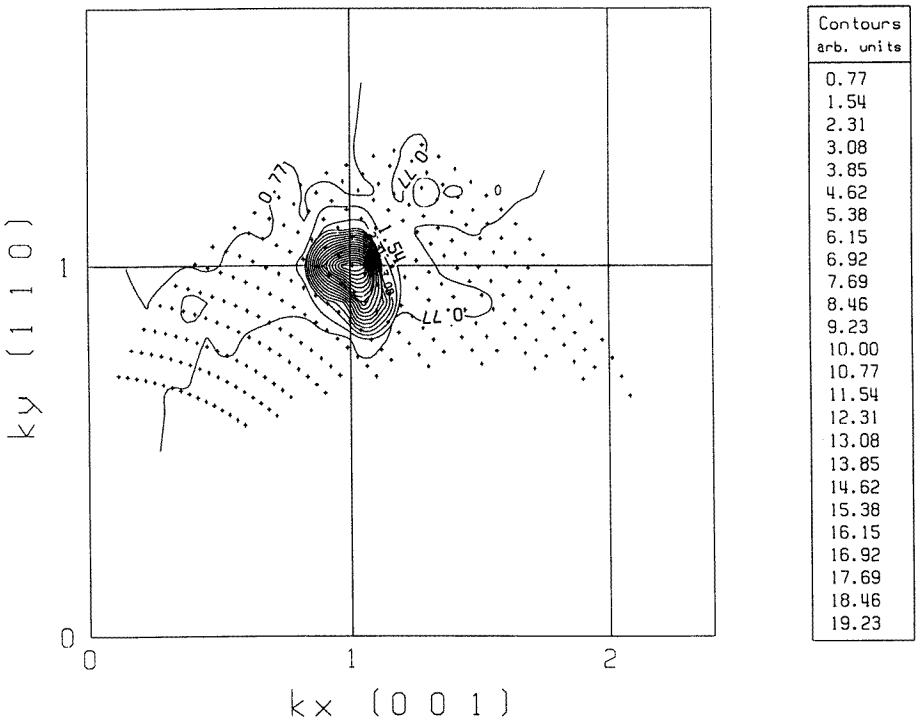

Figure 5. A contour plot of the experimentally determined Fourier transform of the magnetic moment defect distribution, $\mathcal{M}(\boldsymbol{\kappa})$, at 37 K, normalized to a maximum value of 20.0 to enhance the diffuse region.

and for m_1:

$$\begin{aligned}&[x_B^{Fe}x_{A,C}^{Mn}\alpha_{B,(A,C)}^{FeMn}(\boldsymbol{r}) + 2x_{A,C}^{Fe}x_B^{Mn}\alpha_{(A,C),B}^{FeMn}(\boldsymbol{r})]M_B M_{A,C} = -0.1\\ &-0.06M_B M_{A,C} = -0.1\end{aligned} \tag{13}$$

which leads to the following solutions:

$$M_B \equiv \frac{\mathrm{d}M_B}{\mathrm{d}x_B} \sim \pm 4.2(\pm 1.0)\ \mu_B/\text{f.u.} \qquad M_{A,C} \equiv \frac{\mathrm{d}M_{A,C}}{\mathrm{d}x_{A,C}} \sim \pm 0.4(\pm 6)\ \mu_B/\text{f.u.}$$

or

$$M_B \equiv \frac{\mathrm{d}M_B}{\mathrm{d}x_B} \sim \pm 0.4(\pm 6)\ \mu_B/\text{f.u.} \qquad M_{A,C} \equiv \frac{\mathrm{d}M_{A,C}}{\mathrm{d}x_{A,C}} \sim \pm 4.0(\pm 1.0)\ \mu_B/\text{f.u.}$$

The previous results given in the literature and obtained in this study suggest the following as the more reasonable solutions:

$$\frac{\mathrm{d}M_B}{\mathrm{d}x_B} \sim -4.2 \pm 1.0\ \mu_B/\text{f.u.} \qquad \frac{\mathrm{d}M_{A,C}}{\mathrm{d}x_{A,C}} \sim -0.4 \pm 6\ \mu_B/\text{f.u.}$$

The reasons given for the choice of negative sign for solutions at $T = 100$ K also apply here. If it is assumed that $\mathrm{d}M_{A,C}/\mathrm{d}x_{A,C} \sim 0\ \mu_B$/f.u., then $\mathrm{d}M_B/\mathrm{d}x_B \sim -4.1 \pm 0.5\ \mu_B$/f.u.

The above values also compare well (within standard error) with $\mathrm{d}M_B/\mathrm{d}x_B \sim -4.9\ \mu_B$/f.u. and $\mathrm{d}M_{A,C}/\mathrm{d}x_{A,C} \sim 0\ \mu_B$/f.u. deduced from the results given in Yoon's (1975) thesis. The slight discrepancy may be due to the neutron diffraction measurements

of Yoon's (1975) thesis being carried out at 4.2 K whereas in this study they were carried out at 37 K.

The analysis of the results obtained from measurements in both temperature regimes indicate that, within standard error, there is possibly a greater change in the moment difference between Mn and Fe atoms on the B site with change in concentration x_B at $T = 37$ K ($T < T_R$) than at $T = 100$ K ($T > T_R$). This is in agreement with an earlier model proposed by Yoon and Booth (1977) which required a significant change in B site moment as the re-ordering temperature was traversed. The neutron diffraction results have shown the temperature dependence of the change in B site moment coincides with the presence of AFM ordering on the B sublattice below T_R. Thus a possible reason for the larger change in the moment difference between Mn and Fe atoms on the B site with change in concentration x_B below T_R than above T_R may be the AFM alignment of the Mn(B) moments. However, above and below T_R, there does not seem to be much difference between the moments of Mn and Fe atoms on the A, C sites with change in concentration on the A, C sites. That is, the moments of Mn and Fe atoms on A, C sites are very similar, which suggests that Mn atoms replace Fe atoms on the A, C sites with the same moment as that of Fe.

Other Heusler alloys, for example Fe_2VSi and Co_2MnSi, in contrast to Fe_2MnSi, do not exhibit a complex magnetic structure. The compound Fe_2VSi has been previously reported to be weakly paramagnetic (Niculescu *et al* 1977) and Co_2MnSi is a collinear ferromagnet with a larger total moment; its ferromagnetic order remains unchanged down to 4.2 K (Webster 1971). The alloy Fe_2CoSi is also a ferromagnetic material and has a larger value of magnetization than Fe_3Si and Fe_2MnSi (Niculescu *et al* 1977).

5. Conclusion

The average atomic and magnetic moment distributions were determined in the Fe_2MnSi compound. The results above and below T_R indicate a random atomic arrangement with Mn and Fe atoms residing together on each of the A, C and B sites. The Cowley sro parameters are similar at the two temperatures, as is to be expected for nuclear diffuse scattering. Only the individual sro parameter $\alpha^{FeMn}_{(A,C),(A,C)}$ could be determined exclusively and its sign indicates that atoms on A, C sites may not prefer to have atoms from other A, C sites as near neighbours.

A more pronounced negative diffuse scattering in the difference between spin-up and spin-down cross-sections for a $Fe_{2.45}Mn_{0.55}Si$ crystal than for Fe_2MnSi has been observed. The magnetic diffuse scattering results have given a consistent formal description of the magnetic state above and below T_R. In this alloy, the magnetic disturbance produced by Mn atoms is confined to the substituted sites. The change in the moment difference between Mn and Fe atoms on the B site with change in concentration x_B for $T < T_R$ appears to be greater than for $T > T_R$, which is consistent with the results of Yoon and Booth (1977) for observed site moments as a function of concentration. However, above and below T_R, the moments of Mn and Fe atoms on A, C sites are very similar.

Acknowledgments

This work was supported by the Australian Institute of Nuclear Science and Engineering (AINSE) and the Australian Research Council. We would like to thank Dr M F Ling for valuable discussions concerning the theory in this paper.

References

Borie B and Sparks C J Jr 1971 *Acta Crystallogr.* A **27** 198
Cenedese P, Bley F and Lefebvre S 1984 *Acta Crystallogr.* A **40** 228
Cowley J M 1950 *J. Appl. Phys.* **21** 24
Cussen L D, Osborn J C, Gibbs P and Hicks T J 1992 *Nucl. Instrum. Methods* A **314** 155
Davis J R, Cywinski R, Moze O and Hicks T J 1982 *J. Physique Coll.* C7 65
Ersez T, Kennedy S J and Hicks T J 1995a *J. Phys.: Condens. Matter* **7** 8423
Ersez T, Kennedy S J, Kępa H and Hicks T J 1995b *J. Phys.: Condens. Matter* **7** 2593
Hayakawa M and Cohen J B 1975 *Acta Crystallogr.* A **31** 635
Johnson D D, Althoff J D, Staunton J B, Ling M F and Pinski F J 1996 *Nato ASI on the Stability of Materials (Corfu, 1995)* (Dordrecht: Kluwer) at press
Marshall W 1968 *J. Phys. C: Solid State Phys.* **1** 88
Miles J R 1991 *PhD Thesis* Monash University
Niculescu V, Burch T J and Budnick J I 1983 *J. Magn. Magn. Mater.* **39** 223
Niculescu V, Burch T J, Raj K and Budnick J I 1977 *J. Magn. Magn. Mater.* **5** 60
Sears V F 1975 *Adv. Phys.* **24** 1
——1984 Thermal neutron scattering length and cross section for condensed-matter research *Atomic Energy Canada Ltd Report* AECL-8490
Tibbals J E 1975 *J. Appl. Crystallogr.* **8** 111
Watson R E and Freeman A J 1961 *Acta Crystallogr.* **14** 27
Webster P J 1971 *J. Phys. Chem. Solids* **32** 1221
Yoon S 1975 *PhD Thesis* Salford University
Yoon S and Booth J G 1974 *Phys. Lett.* **48A** 381
——1977 *J. Phys. F: Met. Phys.* **7** 1079
Ziebeck K R A and Webster P J 1976 *Phil. Mag.* **34** 973